Cyclic Behavior of Single Angles for Ductile End Cross Frames

LYLE P. CARDEN, FRANCISCO GARCIA-ALVAREZ, AHMAD M. ITANI, and IAN G. BUCKLE

Damage to the superstructures of steel plate girder bridges during past earthquakes (Astaneh-Asl, Bolt, McMullin, Donikian, Modjtahedi, and Cho, 1994; Shinozuka, Ballantyne, Borcherdt, Buckle, O'Rourke, and Schiff, 1995; Bruneau, Wilson, and Tremblay, 1996) has highlighted the need to reduce the effects of transverse seismic loading and, at the same time, indicated a means of achieving this objective with the use of ductile end cross frames (ductile end diaphragms). By designing the cross frames for ductile behavior, the transverse base shear in a bridge can be reduced, minimizing damage to the substructure and other critical superstructure components. Furthermore, confining damage to purpose-built ductile elements that can be easily replaced after an earthquake may reduce the need for bridge closures following a major earthquake.

Single-angle X-braces are often used in cross frames of steel plate girder bridges. It has previously been demonstrated that concentric braces such as these have a tendency toward strength and stiffness degradation due to buckling of the compression members when deformed inelastically (Jain, Goel, and Hanson, 1980; Astaneh-Asl, Goel, and Hanson, 1985). In buildings, this can have serious consequences because the strength degradation has a tendency to form weak stories (Sabelli, 2001), resulting in large deformations concentrated at these levels. Provisions are defined by the AISC *Seismic Provisions for Structural Steel Buildings* (AISC, 2002), hereafter referred to as the AISC *Seismic Provisions*, to minimize the impact of buckling and ensure adequate behavior in special concentrically braced frames. In bridges, it has been shown that when the strength degradation due to buckling is combined with the stiffness of the girders and other components in the transverse load path, the resultant force-displacement envelope of single-angle end cross frames is essentially elasto-plastic (Carden, Itani, and Buckle, 2005a). Therefore, the cross frames act as effective structural fuses, although strength degradation in the overall system is prevented. Hence, as long as the girders and cross frames can accommodate the resulting seismic displacement demand, single-angle X-braces are an effective system for ductile end cross frames.

Lyle P. Carden is a post-doctoral research scholar, department of civil and environmental engineering, University of Nevada, Reno, NV.

Francisco Garcia-Alvarez is an engineer, Garcia Jarque Ingenieros S.C., Del Benito Juarez, Mexico.

Ahmad M. Itani is associate professor, department of civil and environmental engineering, University of Nevada, Reno, NV.

Ian G. Buckle is professor, director of center for civil engineering earthquake research, department of civil and environmental engineering, University of Nevada, Reno, NV.

OBJECTIVES AND SCOPE

The single-angle components designed for end cross frames in bridges are typically much smaller in cross section and have shorter lengths than those used in concentric braced frames in buildings. Therefore, the objective of this paper is to determine, experimentally and analytically, the inelastic cyclic axial behavior of angle braces with properties similar to those proposed for use in ductile end cross frames of steel girder bridges. The angle sizes were at approximately one-half scale compared with those in typical bridges, as they are used in a scale model. The maximum axial deformations, cumulative plastic deformations, and variation in tension and compression capacity are investigated.

EXPERIMENTAL PROGRAM

The single angles used in the cyclic axial experiments were based on the single angles used in experiments on ductile end cross frames in a two-fifths-scale steel girder bridge model (Figure 1) (Carden et al., 2005a). Cyclic axial experiments were performed on 17 single-angle members, with the dimensions of each different configuration shown in Figure 2. Further details of the single angles and their connections used in each experiment are listed in Table 1. Two sizes of single angles were used in the experiments, with sizes that were the same as those used in different cross-frame configurations for the bridge model. The angles came from three different batches of ASTM A36 steel, with ASTM coupon

Table 1. List of Cyclic Axial Single-Angle Experiments

Specimen	Section	Coupon Test	Effective Length (in.)	Gusset Thickness (in.)	Connection (Reinforced)	First Cycle	A_n/A_g	b/t [a]	Kl/r [b]
A	1¾×1¾×¼	1	40.5	½	Bolted	Compression	0.81	7	119
B	1¾×1¾×¼	1	40.5	1	Bolted	Compression	0.81	7	83
C	1¾×1¾×¼	1	40.5	1	Bolted	Tension	0.81	7	83
D	1¾×1¾×¼	1	40.5	1	Bolted (x)	Tension	0.93	7	83
E	1¾×1¾×¼	1	40.5	1	Bolted (c)	Compression	1.00	7	83
F	1¾×1¾×¼	1	22.5	1	Bolted	Compression	0.81	7	46
G	1¾×1¾×¼	1	22.5	1	Bolted	Compression	0.81	7	46
H	1¾×1¾×¼	1	22.5	1	Bolted (x)	Tension	0.93	7	46
I	1¾×1¾×¼	1	22.5	1	Bolted (c)	Compression	1.00	7	46
J	1¾×1¾×¼	2	40.5	1	Welded	Compression	1.00	7	83
K	1¾×1¾×¼	2	40.5	1	Welded	Tension	1.00	7	83
L	1¾×1¾×¼	2	22.5	1	Welded	Compression	1.00	7	46
M	1¾×1¾×¼	2	22.5	1	Welded	Tension	1.00	7	46
N	1×1×x	3	50.5	1	Welded	Compression	1.00	5.33	181
O	1×1×x	3	50.5	1	Welded	Tension	1.00	5.33	181
P	1×1×x	3	25.4	1	Welded	Compression	1.00	5.33	91
Q	1×1×x	3	25.4	1	Welded	Tension	1.00	5.33	91

[a] The limiting b/t ratio for members of special concentrically braced frames in accordance with the AISC *Seismic Provisions* (2002) is 8.5 and for AASHTO (1998) is 12.8, and therefore satisfied by all members.
[b] The limiting Kl/r for special concentrically braced frames based on the AISC *Seismic Provisions* (2002) is 167 and for AASHTO (1998) is 120 for primary members, and therefore satisfied by all members, except Specimens N and O. K = 1.0 for Specimen A and K = 0.7 for the remaining specimens.

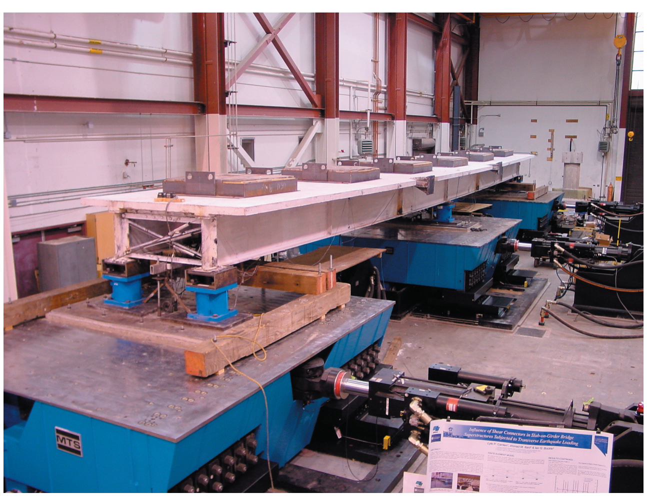

Fig. 1. Bridge model with X-brace end cross frames.

tests performed on a flat bar specimen from each of the three batches. Different lengths were used to represent the full and half lengths of the diagonal members in X-braces, resulting in specimens with different Kl/r and b/t ratios.

Gusset plates, ½ in. thick, were used in the first experiment (Specimen A), which resulted in bending of the gusset plates at each end. It was apparent that the gusset plates were more flexible than those in the bridge model, which were restrained from bending by the top and bottom chords. Therefore, 1.0-in.-thick gusset plates were used for subsequent experiments to promote formation of plastic hinges due to buckling in the angles rather than the gusset plates. This was expected to more accurately represent the behavior in the bridge model.

Some specimens used bolted connections to the gusset plates while other members used welded connections. The bolted members used three different A_n/A_g ratios in the connections. The first was based on the ratio for a member with a line of four bolts through one leg of the angle resulting in an A_n/A_g ratio of 0.81 (Figure 3). In the remaining braces the ratio was increased by reinforcing the connection regions with a plate welded to the connected leg of the single angles, as shown in Figure 4. The members were then bolted through the reinforced section to a gusset plate with resulting A_n/A_g ratios of 0.90 for members reinforced with 3/16 in. plates and 1.0 for members reinforced with 5/16 in. plates. The remaining specimens were welded using balanced welds, whereby the length of the weld on each side of the angle was equal to the inverse of the relative distance from each edge to the centroid of the angle. The balanced welds resulted in the edge at the outstanding leg of the angle being connected with a full-length weld between the gusset plate and the angle, while the other edge was welded along approximately half of this length, as shown in Figure 5. These welds were designed to minimize stress concentrations in the connected leg when axial loads were applied to the member.

Each specimen was subjected to cycles of alternating tension and compression with amplitudes increasing by 0.25 in. increments of displacement, although for some of the specimens, the initial displacement cycle was larger than 0.25 in., as necessary to observe buckling or yielding of the member. Some of the members were first subjected to tensile actions while others were first subjected to compressive actions, as given in Table 1.

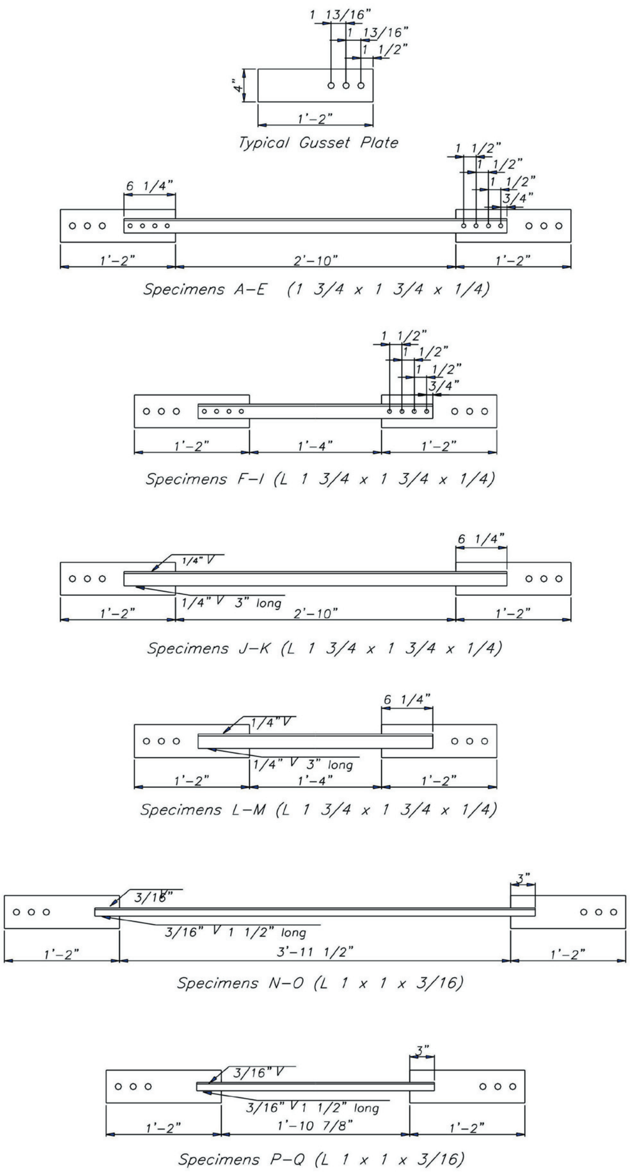

Fig. 2. Single angles used in cyclic axial experiments.

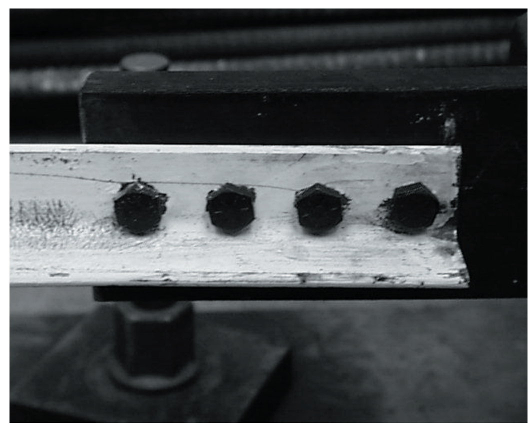

Fig. 3. Four-bolt connection between gusset plate and angle member.

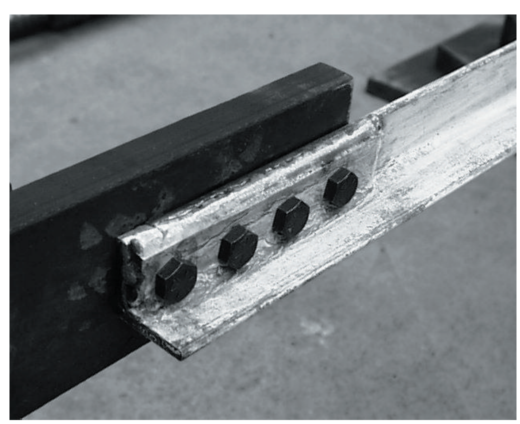

Fig. 4. Bolted connection between gusset plate and angle member with a thickened connected leg in the connection region.

Table 2. Failure Mode, Maximum Effective Axial Strains, and Cumulative Effective Plastic Axial Strains in the Angles

Specimen	Failure Mode	Measured Ultimate Axial Strain (%)	Theoretical Yield Displacement (in.)	Cumulative Effective Plastic Strain (%)
A	At bolt hole	3.1	0.0754	23
B	At bolt hole	4.9	0.0754	77
C	At bolt hole	5.4	0.0754	82
D	At end plastic hinge	6.2	0.0754	127
E	At end plastic hinge	6.2	0.0754	115
F	At bolt hole	5.5	0.0419	52
G	At bolt hole	5.5	0.0419	57
H	At end plastic hinge	8.1	0.0419	127
I	At end plastic hinge	8.9	0.0419	144
J	At midspan plastic hinge	7.4	0.0754	176
K	At midspan plastic hinge	7.7	0.0754	190
L	At end plastic hinge	9.0	0.0419	146
M	At end plastic hinge	8.0	0.0419	128
N	At end plastic hinge	6.0	0.0940	142
O	At midspan plastic hinge	12.2	0.0940	596
P	At end plastic hinge	10.0	0.0473	201
Q	At midspan plastic hinge	7.0	0.0473	113

The experimental assembly used for the single-angle experiments is shown in Figure 6. Axial forces were applied to the members using an actuator that was attached to a slider to ensure pure axial loads. The variation in force due to friction in the slider was measured at less than 1 kip and was neglected in the analysis. Axial displacements and forces were measured by the actuator.

Fig. 5. Welded connection between gusset plate and angle member with balanced welds.

EXPERIMENTAL RESULTS

Hysteretic Behavior of the Angles

Force-displacement traces for each single-angle experiment are shown in Figures 7 through 11. The shape of the observed hysteresis loops is similar for each experiment and comparable to those observed in the past for single and double angles (Jain et al., 1980; El-Tayem and Goel, 1986). In tension, the members yielded followed by a post-yield increase in strength due to cyclic and strain hardening. In compression, the members buckled followed by immediate strength degradation. Stiffness degradation was also observed as the members elongated, resulting in an increased displacement for the same tensile force with successive cycles. The number of cycles that each member was subjected to prior to failure differed with the failure mode for each member (Table 2) and depended largely on the type of connection. Bolted specimens with unreinforced connections each fractured in the region between the edge and first bolt hole of the connected leg, as illustrated in Figure 12. Failure was typically observed much earlier in members with this type of connection than in the other members. With the reinforced bolted connections, which had an increased A_n/A_g ratio, the failure was moved to outside the connection region. Failure in these members occurred in the plastic hinge formed during buckling at either end of the member (Figure 13) with a crack propagating from the edge of the connected leg. The welded connections resulted in an even further improvement in the performance of the angles. These members failed in the plastic hinges formed either at the end of the angle or at midspan as shown in Figure 14. The balanced weld appeared to delay the initiation of cracking at the edge of the connected leg due to an apparently lower stress concentration in this region compared with the bolted connections.

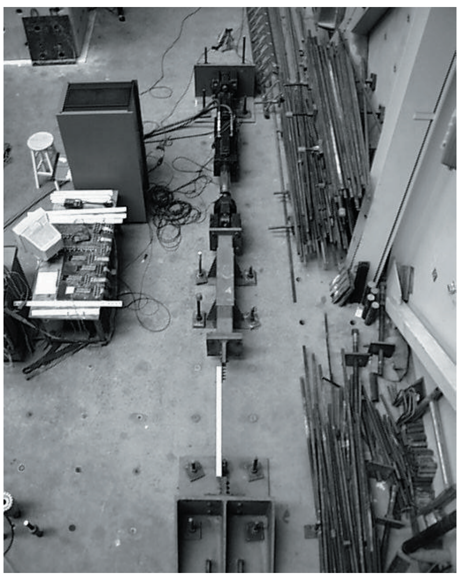

Fig. 6. Experimental setup of cyclic axial experiments on angles.

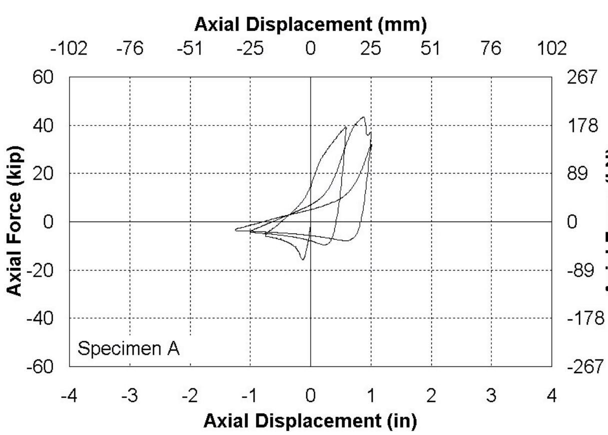

Fig. 7. Force-displacement hysteresis loop for Specimen A (1¾ × 1¾ × ¼ angle connected to ½-in.-thick gusset plates).

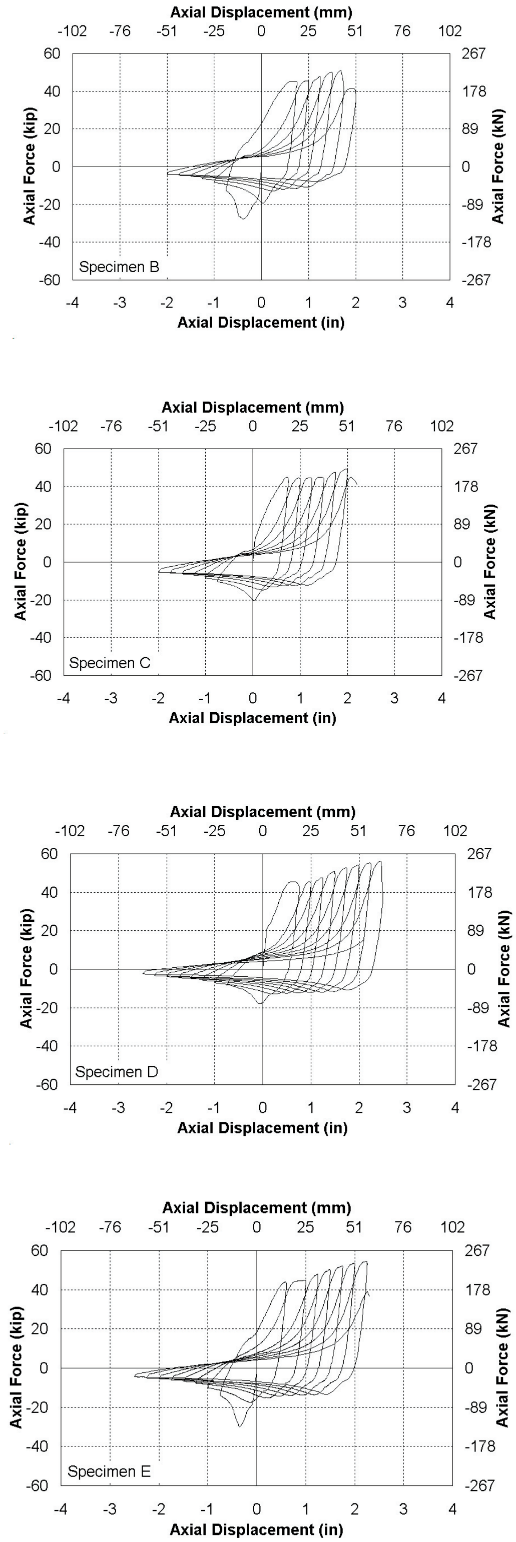

Fig. 8. Force-displacement hysteresis loops for Specimens B through E ("long" bolted 1¾ × 1¾ × ¼ angles connected to 1.0-in.-thick gusset plates).

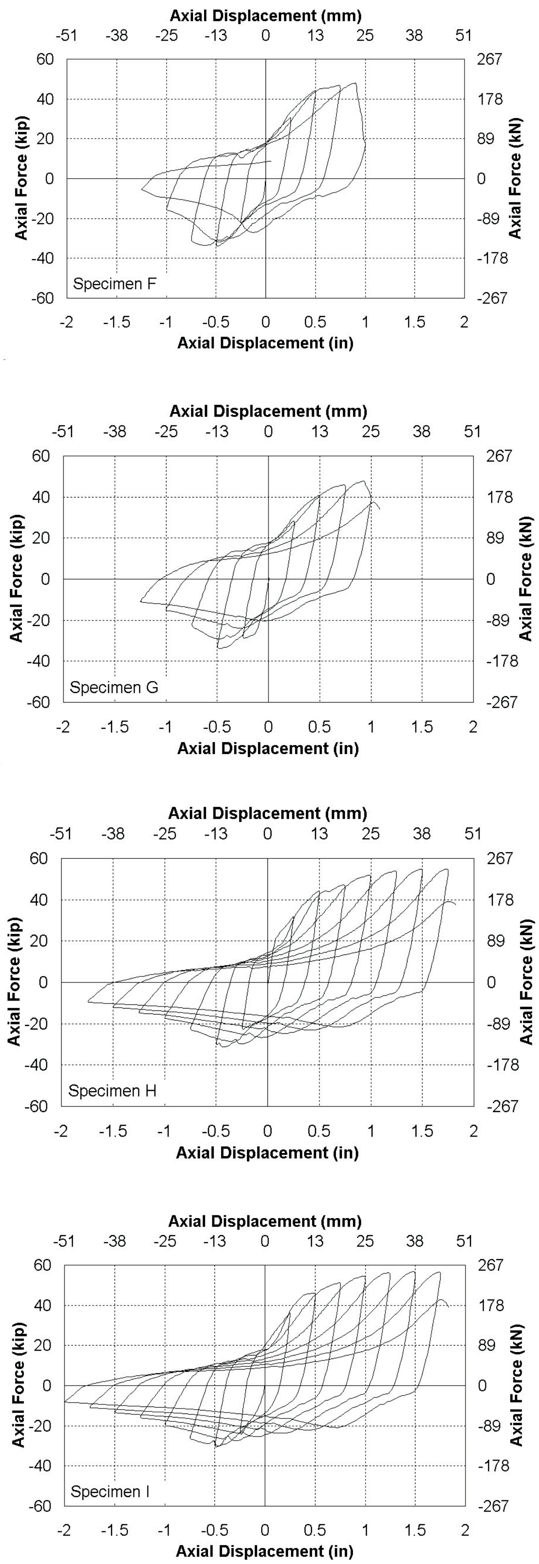

Fig. 9. *Force-displacement hysteresis loops for Specimens F through I ("short" bolted* 1¾ × 1¾ × ¼ *angles connected to* 1.0- *in.-thick gusset plates).*

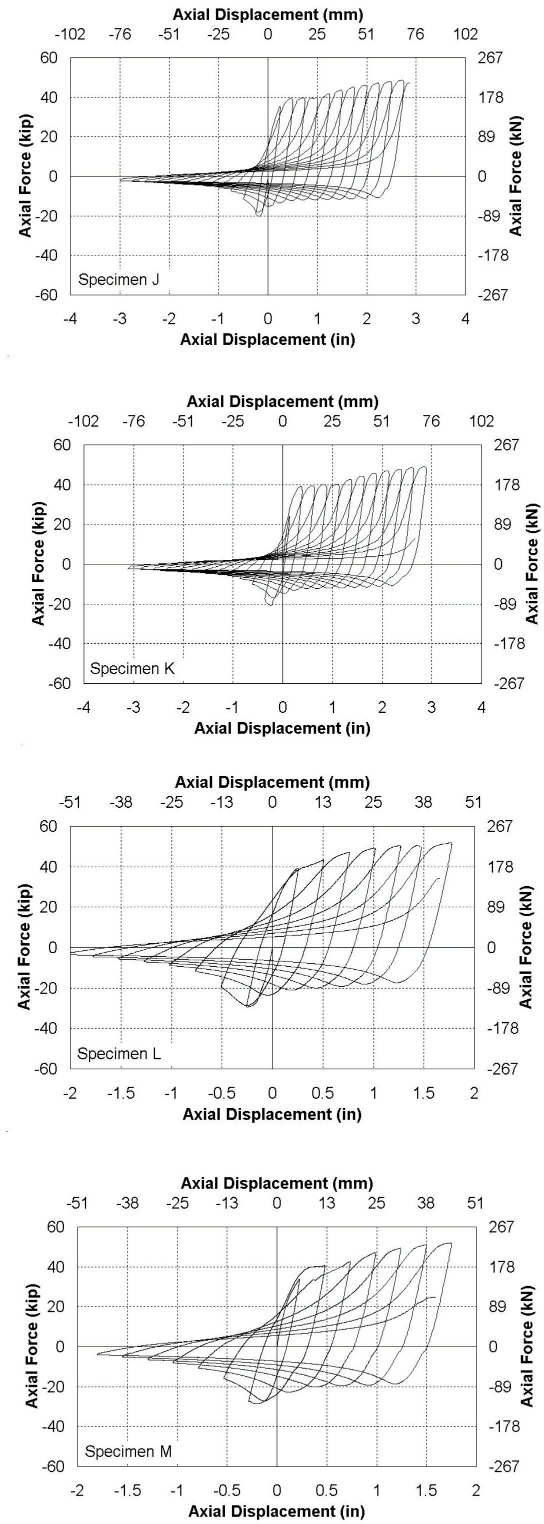

Fig. 10. *Force-displacement hysteresis loops for Specimens J through M (welded "long" and "short"* 1¾ × 1¾ × ¼ *angles with* 1.0-*in.-thick gusset plates).*

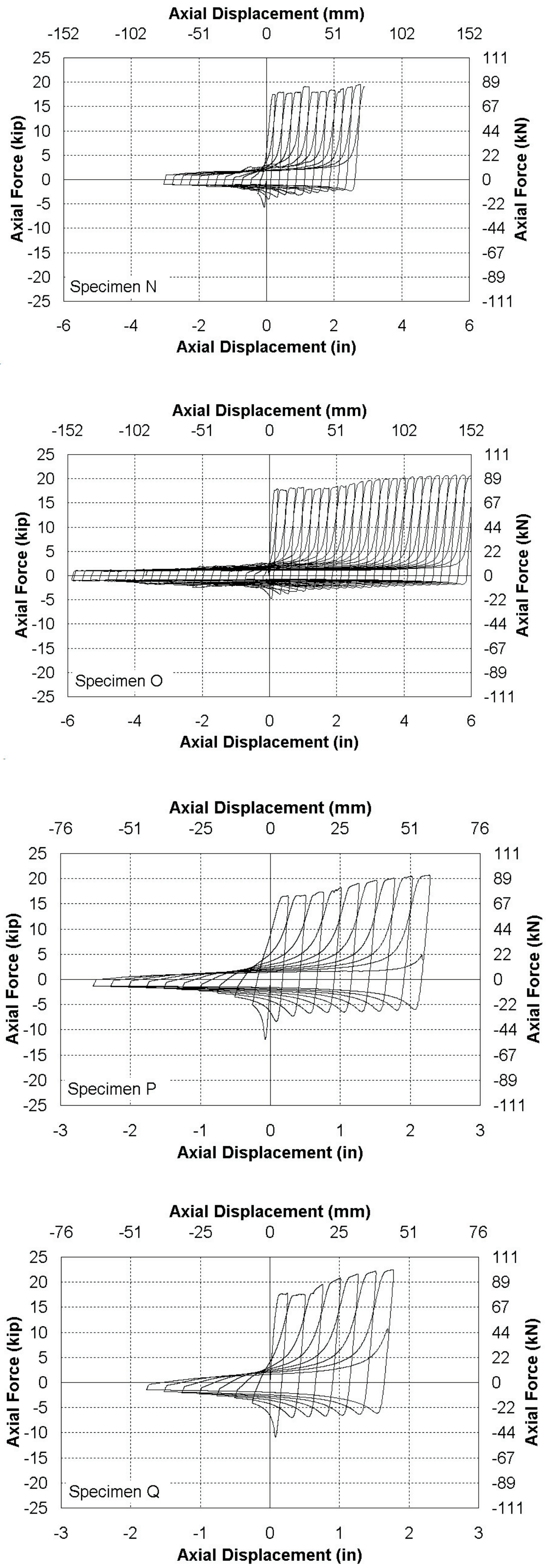

Fig. 11. Force-displacement hysteresis loops for Specimens N through Q (welded "long" and "short" $1 \times 1 \times 3/16$ *angles connected to* 1.0-*in.-thick gusset plates).*

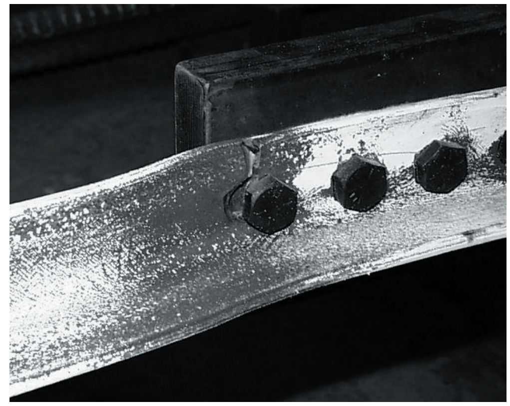

Fig. 12. Fracture of bolted single-angle specimen.

Fig. 13. Fracture of single-angle specimen with thickened bolted connection.

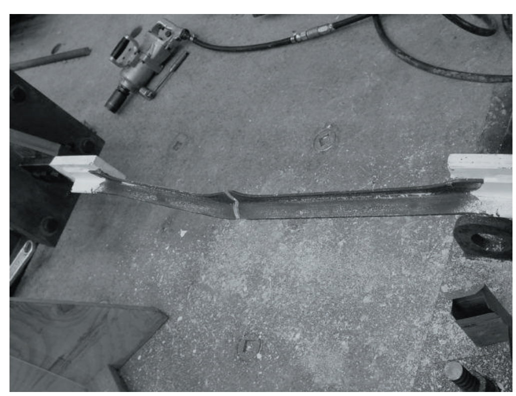

Fig. 14. Fracture of single-angle specimen with welded connections.

Maximum and Cumulative Deformations in the Angles

The maximum average axial strain is used to describe the maximum deformation in each specimen. The average axial strain was calculated using the axial displacement divided by the effective length of the member given in Table 1. This measure of axial deformation, unlike ductility, is independent of the yield displacement, which was shown to depend on the loading history and factors such as slippage in the connections and thus was difficult to determine. The maximum strain is also a useful measure as it can be converted to a maximum drift in X-brace assemblies. Table 2 shows that the maximum effective axial strain for each specimen ranged from 3 to 12%, indicating a large variation in the displacement capacity of the members. Even between theoretically identical members there was up to a 100% difference in their ultimate strains. While there was much variability, distinct factors had an effect on the maximum displacements. An increased A_n/A_g correlated to an increase in displacement due to prevention of premature failure around the bolt holes. For the welded members, and bolted members where fracture was prevented in the connection region using thickening plates, the maximum effective axial strain was at least 6%, while the bolted members where fracture occurred in the connections had a maximum strain below 6%. Thus, thickened bolted connections or welded connections are recommended for the attachment of single angles in ductile end cross frames.

The cumulative plastic strain of each member was calculated to investigate the cumulative plastic deformation capacity. Cumulative plastic strain is defined as the absolute sum of the displacements in excess of the yield displacement divided by the member length for each cycle of deformation in the braces. This is quite different from the true strains in the brace due to the effects of buckling and elongation of the members. In order to define the cumulative plastic strain the yield displacement was calculated based on a theoretical value, Δ_y, given by

$$\Delta_y = \frac{F_{ye} l}{E} \tag{1}$$

where

F_{ye} = expected yield stress, ksi
l = length between the centroid of the connections, in.
E = elastic modulus of the steel member, ksi

The cumulative plastic ductilities for each specimen are given in Table 2. Because of the increasing amplitude loading history, there was a correlation between the maximum strains and the cumulative plastic capacity of the specimens. Those members with fracture observed in their connections resulted in cumulative plastic strains between 23 and 82%. All members for which fracture was prevented in the connections resulted in cumulative plastic strains between 113 and 201%, with the exception of Specimen O, which had an unusually high cumulative plastic strain of 596%. This was one of two members that violated the *Kl/r* limit of 120, which may explain the large cumulative strain as the buckled behavior was largely elastic resulting in less cyclic plastic deformation in the members, particularly localized deformation in the plastic hinges. Less localized plastic deformation allowed the member to undergo a larger number of cycles; however, it made the member less effective as an energy dissipator than one that undergoes inelastic buckling. Furthermore, the slender properties resulted in a large variability in response as illustrated when Specimen O is compared with the theoretically identical Specimen N (Figure 11). The average cumulative strain for members without connection fracture, neglecting Specimen O, was 146%.

From these experiments it is recommended that single-angle members in ductile end cross frames should be designed for a maximum deformation during an earthquake not exceeding 4.0%. Therefore, for the maximum considered earthquake, a strain of no more than 6.0%, 1.5 times the design-level earthquake, would be expected. This is consistent with the design of an isolation system, which should be stable up to 1.5 times the design displacement (AASHTO, 1999) and also the buckling-restrained braced frame guidelines, which state that a brace should be capable of withstanding building drifts up to 1.5 times the design drift (SEAONC, 2003). The maximum strain limit of 6.0% is less than that for any of the members where fracture was avoided in the connection region, using thickened plates with bolted connections or balanced welded connections.

The X-braces in the bridge model during shake table experiments were not deformed up to strains of 6.0% as in the cyclic experiments, as other factors such as allowable girder drifts limited the bridge displacements. Therefore, an analytical model of the bridge model (Carden, Itani, and Buckle, 2005b) was used to theoretically estimate the cumulative plastic strains in the braces for a series of different earthquakes, scaled to result in a 6.0% maximum strain in the braces. The resulting cumulative plastic strains for 10 different earthquake excitations are listed in Table 3. The average cumulative plastic strain was 70%, and the mean plus one standard deviation level of cumulative plastic strain was 110%. This is approximately equal to the most conservative value of the cumulative plastic strain (113%) measured in the axial experiments for the specimens that utilized the recommended connection details; therefore, 6.0% maximum strain is considered an appropriate level for the maximum credible earthquake. Similarly, 4.0% strain is appropriate for the design-level earthquake. This design value was exceeded even by the members with poor connection detailing, except Specimen A, and therefore is conservative for well-detailed

Table 3. Cumulative Plastic Strains and Ductilities in Analytical Model for Different Earthquakes Subjected Braces to 6.0% Strain

Earthquake	Station and Component	Amplitude Scale Factor	Maximum Brace Strain (%)	Cumulative Plastic Strain (%)	Cumulative Plastic Ductility
1940 Imperial Valley	El Centro Array#9 NS	5.10	5.98	136.2	633
1966 Parkfield	California Array#2 NS	3.20	6.01	80.0	372
1971 San Fernando	Pacoima Dam NS	2.00	5.86	52.9	246
1977 Bucharest	Building Res. Inst. NS	3.80	5.88	32.3	150
1979 Imperial Valley	Array #7 230°	3.00	5.95	68.0	316
1992 Landers	Lucerne EW	3.00	5.84	28.2	131
1994 Northridge	Sylmar Hospital NS	2.40	6.08	49.7	231
	Rinaldi S49W	1.25	5.89	44.3	206
1995 Kobe	KJMA NS	1.65	5.98	67.3	313
1999 Taiwan Chi-Chi	TCU084 EW	0.90	6.22	143.0	665
Average =			5.97	70.2	326
Average + 1 Standard Deviation =			6.08	110.1	512

members. For 36 ksi steel, this corresponds to a theoretical axial ductility of 32, and for 50 ksi steel, an axial ductility of 23.

Tensile Yield Strength

Tests were performed on coupons taken from single-angle members of the same heat numbers as the members used in the bridge model in accordance with the ASTM A370 standard coupon test for flat bars. Test 1 was for the heavy single angles with bolted connections, Test 2 was for the heavy single angles with welded connections, and Test 3 was for the light single angles. Each set of angles came from a different heat number. The yield strengths from the three tests were 55, 27, and 36% larger, respectively, than the minimum specified strength of 36 ksi for the ASTM A36 steel members. The ultimate strength was 50 to 52% larger than the measured yield stress for each specimen, and the elongation at fracture was between 30 and 35% for each specimen.

The tensile yield point for the single-angle specimens is defined as the point where the entire member yields. For a concentrically loaded member subjected to monotonic axial loads, this point can be clearly identified using such limits as the force at 0.2% offset strain. However, for the single-angle members subjected to cyclic loads, it was more difficult to identify the yield point, first, because there was an eccentricity in the connection between the single angles and the gusset plates with the resulting moment causing part of the member to yield before the entire member yielded. Second, there was slippage in the bolted connections that resulted in additional axial displacement, effectively reducing the stiffness of the member prior to yielding. In addition, some of the members buckled in compression before being subjected to tension; hence the properties of these members were modified by the formation of a plastic hinge due to buckling. These factors made it impossible to use a consistent method to identify the yield point. The yield point was subsequently identified by inspection at the point where the yield plateau was observed, indicating that the entire member had yielded. The yield strength was relatively insensitive to variation in selection of the yield point and prior loading history. The estimated yield forces for each experiment are summarized in Table 4.

In order to compare the measured yield and ultimate strengths to predicted values, the nominal yield forces, expected yield strength based on the material strength from coupon tests, and the expected yield strength based on AISC (2002), were each calculated. The nominal tensile strength is given by (AASHTO, 1998; AISC, 2005)

$$P_{ny} = F_y A_g \tag{2}$$

where

P_{ny} = nominal yield strength, kips
F_y = nominal yield stress of the material, ksi
A_g = gross area of the section, assuming the connections are designed to prevent net section fracture, in.^{2}

Table 4. Tensile and Compressive Strengths of Single-Angle Specimens Compared with Expected Properties

Spec.	Tensile Strength					Compressive Strength		
	Measured Yield Strength (kips)	Measured Ultimate Force (kips)	Nominal Yield Force (kips)	Yield Force Coupon Tests (kips)	Expected Yield Strength (kips)	Measured Buckling Strength (kips)	Calculated Buckling Force 1[b] (kips)	Calculated Buckling Force 2[c] (kips)
A	[a]	43.4	29.3	45.5	43.9	15.9	12.2	14.3
B	44.9	50.8	29.3	45.5	43.9	27.7	12.2	25.8
C	44.6	49.2	29.3	45.5	43.9	20.4	12.2	25.8
D	44.8	56.0	29.3	45.5	43.9	17.8	12.2	25.8
E	43.8	54.6	29.3	45.5	43.9	29.9	12.2	25.8
F	45.2	47.8	29.3	45.5	43.9	33.7	18.8	38.2
G	45.1	47.7	29.3	45.5	43.9	33.9	18.8	38.2
H	45.0	54.9	29.3	45.5	43.9	31.3	18.8	38.2
I	44.8	56.8	29.3	45.5	43.9	30.5	18.8	38.2
J	38.5	48.6	29.3	37.2	43.9	20.2	12.2	23.4
K	38.6	49.2	29.3	37.2	43.9	20.8	12.2	23.4
L	40.0	51.9	29.3	37.2	43.9	28.5	18.1	32.3
M	40.2	52.0	29.3	37.2	43.9	28.7	18.1	32.3
N	16.3	18.6	12.2	16.7	18.4	6.3	1.4	2.6
O	17.4	20.8	12.2	16.7	18.4	4.6	1.4	2.6
P	16.6	20.7	12.2	16.7	18.4	12.0	4.4	9.2
Q	17.6	22.5	12.2	16.7	18.4	10.7	4.4	9.2

[a]Yield strength not clearly identified.
[b]Calculated based on AISC specifications (2005) with K = that calculated from Section E5(a)
[c]Calculated based on AISC specifications (2005) with K = 1.0 for Specimen A (plastic hinges observed in gusset plates) and 0.7 for all other specimens (plastic hinges observed in angles).

The expected yield strength based on the material strength from coupon tests was calculated by using the actual yield strength of the material from the coupon tests instead of the minimum specified strength in Equation 2. The expected yield strength based on AISC (2002) was calculated by multiplying the nominal strength by an R_y factor of 1.5 as specified for ASTM A36 steel. Each of these predicted values are given in Table 4. This table shows that the expected yield strength based on coupon tests was within 7% of the measured yield strength. The expected yield strength based on AISC (2002) was typically within 10% of the measured yield strength with a maximum difference of 14%. Therefore, while coupon tests are useful to accurately define the expected yield strength, the R_y factor resulted in a good estimate for these members. In all cases, the strength of the members was above their minimum specified values. The ultimate force or maximum force measured in each specimen was, on average, 21% larger than their measured yield strength, with the maximum difference being 28%.

Buckling Capacity

The buckling capacity, or maximum compression force, for each specimen is listed in Table 4. The buckling capacity was dependent on the material properties, cross-sectional properties, effective length of the members, and the loading history with members subjected to prior tensile yielding typically having a reduced buckling capacity. The buckling capacity, P_{nc}, was predicted using AASHTO (1998) [equivalent to AISC (2005)], for the slenderness parameter, λ, greater than 2.25, by

$$P_{nc} = 0.66^{\lambda} F_y A_g \tag{3}$$

where the slenderness parameter is given by

$$\lambda = \left(\frac{Kl}{r\pi}\right)^2 \frac{F_y}{E} \tag{4}$$

where

K = effective length factor
r = radius of gyration about the minor principal axis of the angle, in.

The effective length was dictated by the end conditions. In practice there are two types of end conditions that exist. The first is where plastic hinging due to buckling is expected in the gusset plates, such as for the detail shown in Figure 15a. The second condition is where plastic hinging will occur in the angles, for example, as in the detail in Figure 15b, where the stiffener will be restrained by welds to the web and flange, or in Figure 15c, where a bottom chord, which will typically be used in new bridges, will prevent bending of the gusset plate. The position of the plastic hinge is based on the relative stiffness and flexural strength of the connecting plate and angle members. In most practical cases, the location of the plastic hinges can be determined by inspection of the connection based on the conditions described above. For Specimen A, connected to 0.5-in.-thick gusset plates, plastic hinging due to buckling was observed in the gusset plates. For the remaining specimens, with the 1.0-in.-thick gusset plates to simulate the condition where the gusset plates are restrained to prevent bending, plastic hinging was observed in the angle members. While concentric braced frames are typically designed to allow hinging in the gusset plates due to buckling, comparison of Specimens A and B (Table 4) shows that a rigid gusset plate, causing a plastic hinge in the end of the angle, resulted in a larger displacement and cumulative displacement capacity.

In the past, attempts have been made to quantify the effective length factor based on the relative stiffness of gusset plate components (El-Tayem and Goel, 1986; Astaneh-Asl et al. 1985). El-Tayem and Goel suggested that an effective length factor of 0.85, with the length defined by the full length of the angles, is appropriate for typical single-angle X-brace members with simple gusset plate connections. In that study, the plastic hinges that formed during buckling of the members, occurred in the gusset plates. In the AISC *Specification for Structural Steel Buildings* (AISC, 2005), equations are given for calculating the effective length factor for single-angle members. Using these equations, the calculated capacity of each of the angle members in the current study was determined. The calculated forces assumed that the length of the elements was defined between the centroids of the connections and was based on the yield strengths from coupon tests. The resulting buckling forces are given in Table 4 (Calculated Buckling Force 1). However, compared with the experimental data, the calculated buckling forces are shown to be conservative, with estimated capacities of between 31% and 77% of the measured capacity. The effective length factor used in these calculations was derived for truss members, assuming some rotation at the ends allowed by torsion in the chords of the truss, assumptions that are not suitable for the experiments described in this paper.

In a second estimate of the buckling force, an effective length factor of 1.0 was assumed when the plastic hinge due to buckling occurred in the gusset plate. This is comparable to an effective length factor of 0.85 using the full length of the member and thus is similar to the assumption of El-Tayem and Goel (1986). Alternatively, when gusset plates were sufficiently rigid or restrained, resulting in plastic hinges in the

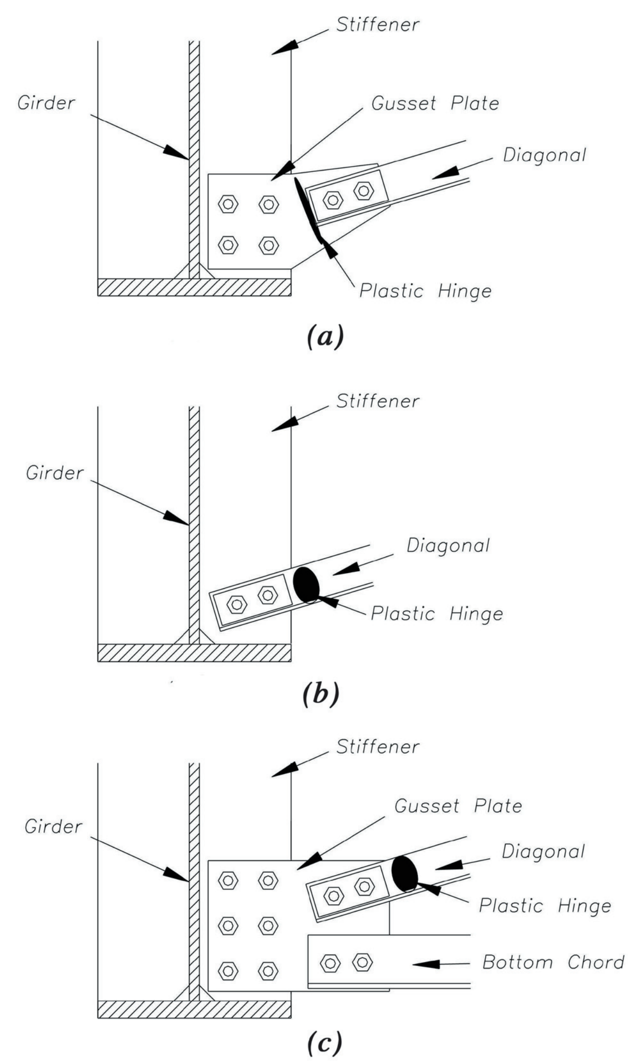

Fig. 15. Different connection configurations for diagonal members of ductile end cross frames.

angles, an effective length factor of 0.7 was assumed. The resulting calculated buckling capacity for each specimen is given in Table 4. For specimens not affected by prior tension yielding, the measured buckling strengths were within 20% of the calculated strengths. As the buckling force was a relatively small part of the overall strength of an X-brace, a 20% error in buckling force correlated to a 5 to 10% error in the overall X-brace strength. Specimen N was the one member first subjected to compression that had a measured strength that differed from the calculated strength by more than 20%. This was also one of two slender members with a *Kl/r* ratio of 181. All other members have a *Kl/r* ratio of less than 120. The larger error that is loosely correlated to a larger *Kl/r* ratio may be explained by the influence of bending caused by the eccentricity between the centroid of the angle and plane of the connection. For slender members the buckling capacity is more sensitive to the effects of bending and the lateral deformation that results.

Comparison between the members first loaded in tension and those first loaded in compression shows that prior tensile loading typically reduced the buckling capacity of the members by about 20%. This is also attributed to the eccentricity in the axial loading of an angle that induces a bending moment in the angle if first loaded in tension, which results in a small lateral deformation and initiation of some plastic behavior in the ends of the angle. This lateral deformation subsequently lowers the buckling capacity of the member during a compression cycle when the loading is reversed. Again the largest difference between the buckling capacities in the members first loaded in tension or compression is observed in the most slender members.

Specified slenderness and width-thickness ratios must also be checked. It is recommended that the cross frame members, being primary members for seismic loading, use the AASHTO (1998) *Kl/r* ratio limit of 120. This will prohibit the use of slender members such as Specimen N and O that have buckling strengths that are sensitive to the effective length and prior loading. The *b/t* ratios defined by the AISC *Seismic Provisions* (2002) for special concentrically braced frames should also be satisfied to prevent local buckling as this is known to have a detrimental effect on the cyclic performance of steel members. In all cases, these limits were satisfied by the angles in this study.

Energy Dissipation in the Single Angles

The area enclosed by each cycle of the hysteresis loops was calculated using a simple algorithm for each specimen and was divided by the rectangular area enclosed by the maximum positive and negative forces and displacements to give the hysteretic area as a ratio of that for an "ideal" system. Analyses of the data show that early cycles have hysteretic energy dissipation of typically 40% of the "ideal" hysteretic area, while for subsequent cycles the equivalent energy dissipation is sometimes reduced to below 20% prior to failure (Figure 16). The reduction in energy dissipation can be explained by considering the two primary sources of hysteretic behavior. The first is tensile plastic elongation with increasing amplitude positive displacements. This member elongation was largely irrecoverable and essentially only contributed to dissipating energy when positive displacement amplitudes exceeded previous amplitudes. The elongation resulted in pinched hysteresis loops and, consequently, a decrease in energy dissipation with repeated cycles. This property causes the amount of energy dissipation for a given cycle to be dependent on the prior loading history. The second, more minor, source of hysteretic energy dissipation in these types of members is from the plastic hinges formed during buckling of the members. The axial force resisted by plastic hinges is dependent on the displacement in the specimen, degrading as displacements increase in compression. Figure 16 shows that the members with the larger slenderness ratios (*Kl/r*) have smaller energy dissipation ratios, which supports limiting the slenderness ratio to 120 as discussed in the previous section.

ANALYTICAL MODEL OF SINGLE-ANGLE MEMBERS

To compare the single-angle X-braces with other ductile systems, an analytical model of the single-angle components was developed with focus on Specimens P and Q, as these had the properties closest to those used in experiments on the bridge model with ductile X-braces. Therefore, a model of these specimens was developed using kinematic NLLink elements in SAP2000 v8.30 (Computers and Structures, 2003), and was designed to capture the tension force envelope, compression force envelope, hysteretic energy per cycle, and the loading history dependent properties. The model

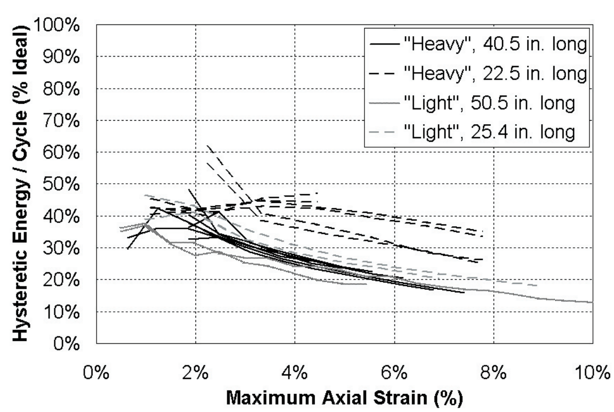

Fig. 16. Energy dissipated per cycle as a percentage of "ideal" for single-angle specimens.

was developed using two NLLink elements in parallel. The first element essentially captured the compression envelope, where the force-displacement curve in compression was based directly on the envelope for Specimen P (subjected to compression on the first cycle). The maximum buckling force was 12.0 kip. The first element had assumed elasto-plastic tension properties with a yield force equal to 2.0 kip. This constant tension force allowed for the residual force in the member as it straightened after a compression buckling excursion due to plastic hinging in the member. In reality this is not a constant force and is dependent on the out-of-plane displacement of the buckled member; however, a constant value of 2.0 kips resulted in an approximately equivalent hysteretic area. The second NLLink element captured the remaining tension properties allowing for pinching due to elongation of the member using the kinematic model. This had elastoplastic tensile properties with a yield force of 17.1 kips, determined by equating areas between the elastoplastic model and average envelope between Specimens P and Q, and a nominally small elastic stiffness in compression. By modeling the element in this way, the tension properties were activated only once when the tensile displacement exceeded that from previous cycles. The overall yield force was equal to 19.1 kips, which compared to within 4% of the expected value of 18.4 kips. This model was the basis for the model described earlier that was used to calculate cumulative plastic strains in braces in the bridge model when excited with different earthquakes.

Importing the loading histories into the analytical model from the experiments for Specimens P and Q, respectively, the hysteresis loops for the nonlinear elements are shown in Figures 17 and 18. These figures show that the models fit the complex hysteretic shape of the single angles relatively well and the maximum tensile and compressive forces were captured. One area of inaccuracy is at the start of a compression cycle. The model for the compression element assumes that the member will degrade in strength at a defined absolute compression displacement. Therefore, any tensile deformation will be recovered assuming an elastoplastic response until the compression displacement reaches a point at which degradation in strength starts to occur. This is noticeable after the first cycle in Figure 18. This inaccuracy could be overcome with the use of a hook element in series with the compression element; however, the model becomes computationally much less efficient and was found to not result in significantly better accuracy.

While this model is effective for nonlinear time history analysis, it is of little use in design and requires calibration to experimental data. A recommended design procedure for ductile end cross frames in bridges (Carden et al., 2005b) based on a capacity spectrum analysis proposes the use of bilinear approximations for the ductile response. Two elasto-plastic bilinear approximations are considered to calculate the maximum force and displacement responses, respectively. The first bilinear response considers the tensile yield force combined with the maximum buckling force. The second bilinear approximation considers the tensile yield force combined with 30% of the buckling force to account for degradation in strength, as illustrated in Figure 19. The 30% compression force is consistent with the AISC *Seismic Provisions* (AISC, 2002) for special concentrically braced frames when calculating unbalanced forces. It is also used in the design of the ductile components of special truss moment frames (AISC, 2002; Goel and Itani, 1994). As the actual response of a given cycle of deformation in the angles is not typically elastoplastic, resulting in reduced energy dissipation compared with that calculated for an equivalent elastoplastic hysteresis loop, a damping reduction factor should be considered. Further details are provided by Carden et al. (2005b). These equivalent models are able to

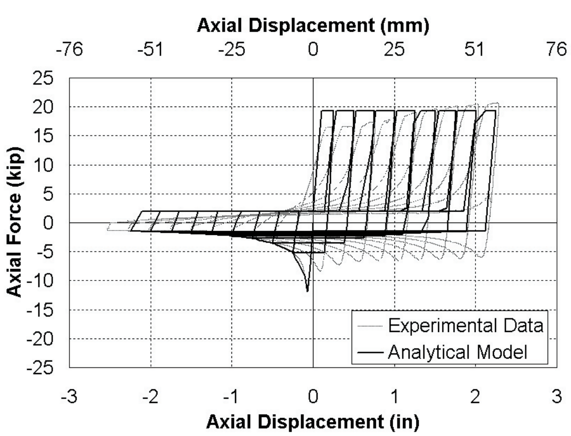

Fig. 17. Analytical model of single-angle compared with experimental data for Specimen P.

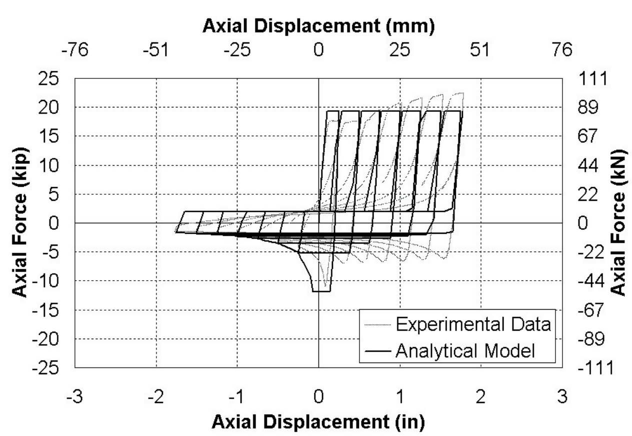

Fig. 18. Analytical model of single-angle compared with experimental data for Specimen Q.

capture the maximum force and displacement in a system with single-angles as the main ductile elements.

CONCLUSION

The cyclic inelastic behavior of single-angle specimens with dimensions typical of those used for the diagonals of X-braces in bridge cross frames, at half scale, has been described. It was shown that angles can be designed to achieve a ductile response with large inelastic strains prior to failure. Failure of single angles is dictated by the properties of the connections, such that bolted connections with an A_n/A_g ratio of 0.81 failed with limited axial ductility due to fracture around the bolt holes. Using a thickening plate to increase the A_n/A_g ratio and move fracture of the specimen to outside the connection region resulted in improved cyclic behavior. Connections with balanced welds between the angles and gusset plates exhibited the most favorable cyclic behavior with the largest maximum strain and cumulative plastic strain. For members where failure was prevented in the connections, the resulting maximum strains are greater than 6% and effective cumulative plastic strains are greater than 113%.

Tensile yield forces in the single angles were within 7% of the calculated capacity based on material strength from coupon tests. The expected yield strengths, based on an R_y factor from AISC (2002), were typically within 10% of those measured. Buckling capacity is dependent on the effective length of the members which, in turn, is dependent on the type of end conditions. Where plastic hinging is expected in the gusset plate, an effective length factor of 1.0 can be assumed for the member. In contrast, where plastic hinging is expected in the member, an effective length factor of 0.7 is appropriate, where the length is defined as the distance between the centroids of the connections. It is recommended that Kl/r be limited to 120 to prohibit the use of slender members for which the buckling strength is sensitive to effective length. By limiting the slenderness ratio to 120, the members are treated like main members for seismic loads based on AASHTO (1998) and the b/t ratio should be limited to those specified for special concentrically braced frames (AISC, 2002). The energy dissipation in single angles decreases upon repeated load cycles, due to degrading stiffness. Corresponding hysteresis loops have areas typically between 20 and 40% of the circumscribing rectangular area, with the level being dependent on the loading history. An analytical model was able to simulate the cyclic, nonlinear, time history response of the single angles. For design purposes, two elastoplastic bilinear models are considered sufficiently accurate to calculate expected maximum force and displacements, respectively, in a system with single-angle braces.

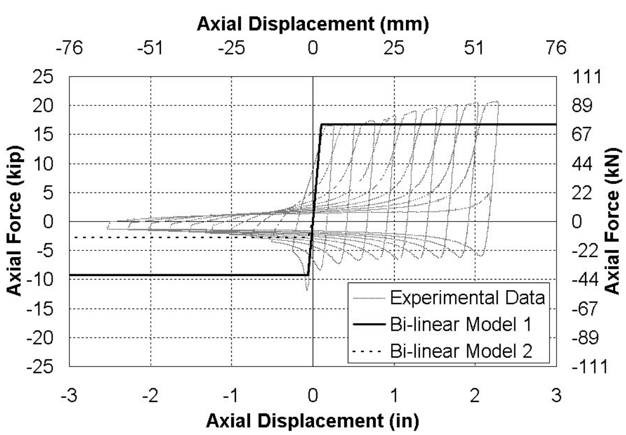

Fig. 19. Bilinear elastoplastic models for envelope of single-angle compared with experimental data for Specimen P.

ACKNOWLEDGMENTS

This project was funded by the California Department of Transportation under contract 59Y564. Additional funding was provided by the Federal Highway Administration through the Highway Project at the Multidisciplinary Center for Earthquake Engineering, University of Buffalo under contract DTFH61-98-C-00094. Grateful acknowledgment is made of both agencies for their generous support.

REFERENCES

AASHTO (1998), *LRFD Bridge Design Specifications*, Customary U.S. Units, 2nd Ed., American Association of State Highway and Transportation Officials, Washington, DC.

AISC (2002), *Seismic Provisions for Structural Steel Buildings*, ANSI/AISC 341, American Institute of Steel Construction, Inc., Chicago, IL.

AISC (2005), *Specification for Structural Steel Buildings*, ANSI/AISC 360, American Institute of Steel Construction, Inc., Chicago, IL.

Astaneh-Asl, A., Goel, S.C., and Hanson, R.D. (1985), "Cyclic Out-of-Plane Buckling of Double Angle Bracing," *Journal of Structural Engineering*, Vol. 111, No. 5, pp. 1135–1153.

Astaneh-Asl, A., Bolt, B., McMullin, K.M., Donikian, R.R., Modjtahedi, D., and Cho, S. (1994), *Seismic Performance of Steel Bridges During the 1994 Northridge Earthquake*, UCB/CE-STEEL-94/01, Department of Civil Engineering, University of California at Berkeley, Berkeley, CA.

Bruneau, M., Wilson, J.W., and Tremblay, R. (1996), "Performance of Steel Bridges during the 1995 Hyogoken-Nanbu (Kobe, Japan) Earthquake," *Canadian Journal of Civil Engineering*, Vol. 23, No. 3, pp. 678–713.

Carden, L.P., Itani, A.M., and Buckle, I.G. (2005a), *Seismic Performance of Steel Girder Bridge Superstructures with Ductile End Cross Frames and Seismic Isolation*, CCEER 05-04, University of Nevada–Reno, Reno, NV.

Carden, L.P., Itani, A.M., and Buckle, I.G. (2005b), *Analysis and Design of Steel Plate Girder Bridges for Transverse Seismic Loads*, CCEER 05-12, University of Nevada–Reno, Reno, NV.

Computers and Structures (2003), *SAP2000 Nonlinear (Version 8.3.0): Structural Analysis Program*, Computers and Structures, Inc., Berkeley, CA.

El-Tayem, A. and Goel S.C. (1986), "Effective Length Factor for the Design of X-Bracing Systems," *Engineering Journal*, AISC, Vol. 23, 1st Quarter, pp. 41-45.

Goel, S.C. and Itani, A.M. (1994), "Seismic Resistant Special Truss Moment Frames," *Journal of Structural Engineering*, ASCE, Vol. 126, No. 6, pp. 1781–1797.

Jain, K.A., Goel, S.C., and Hanson, R.D. (1980), "Hysteretic Cycles of Axially Loaded Steel Members," *Journal of the Structural Division*, ASCE, Vol. 106, No. 8, pp. 1777–1797.

Sabelli, R. (2001), *Research on Improving the Design and Analysis of Earthquake-resistant Steel-braced Frames*, PF2000-9–FEMA/EERI 2000 Professional Fellowship, Oakland, CA.

SEAONC (2003), *Recommended Provisions for Buckling-Restrained Brace Frames*, Structural Engineering Association of Northern California, Sacramento, CA, July.

Shinozuka, M. (ed), Ballantyne, D., Borcherdt, R., Buckle, I., O'Rourke, T., and Schiff, A. (1995), *The Hanshin-Awaji Earthquake of January 17, 1995 Performance of Lifelines*, NCEER-95-0015, National Centre for Earthquake Engineering Research, Buffalo, NY.